Molecular Vision 2026; 32:102-118 <http://www.molvis.org/molvis/v32/102>
Received 3 October 2025 | Accepted 18 February 2026 | Published 20 February 2026

RNA interference to reduce *Egr1* expression in rods delays retinal degeneration in a model of retinitis pigmentosa

Luca Merolla,[1] Antonia Fottner,[1] Cornelia Imsand,[1] Claudia Matter,[1] Jessica Rowlan,[2] Maureen Neitz,[2] Larissa P. Govers,[1] Marijana Samardzija,[1] Christian Grimm[1]

[1]Laboratory for Retinal Cell Biology, Department of Ophthalmology, University Hospital Zurich, University of Zurich, Zurich, Switzerland; [2]University of Washington, Department of Ophthalmology, Seattle, WA

Purpose: Retinitis pigmentosa (RP) is a heterogeneous group of inherited retinal diseases characterized by progressive photoreceptor degeneration. The early growth response-1 gene (*Egr1*) is an immediate-early gene implicated in neurodegenerative and stress responses in the retina, among many other tissues. While its expression is induced in the retina across various RP models, its functional role in the degenerative process remains unclear. This study aimed to investigate the contribution of *Egr1* to photoreceptor degeneration in vivo.

Methods: We used adeno-associated virus (AAV)-mediated RNA interference and transgenic overexpression to modify *Egr1* levels in rod and cone photoreceptors of wild-type and *Rho*$^{P23H/+}$ mice. Rod- and cone-specific promoters enabled cell-specific expression. Exposure to high levels of white light was used to induce retinal degeneration in wild-type mice. We assessed retinal structure and transgene expression through funduscopy, optical coherence tomography (OCT), immunofluorescence, and histological analysis. We measured *Egr1* mRNA expression levels via real-time PCR and assessed the effects of *Egr1* modulation on the retina by determining the thickness of the outer nuclear layer (ONL) and the number of surviving cones.

Results: Similar to other models of retinal degeneration, *Egr1* was induced in the retina after light exposure and in the *Rho*$^{P23H/+}$ mouse during degeneration. AAV-mediated down- or upregulation of *Egr1* in rods or cones did not affect retinal morphology in wild-type mice. In *Rho*$^{P23H/+}$ mice, *Egr1* knockdown in rods modestly preserved ONL thickness up to 12 weeks after AAV injection. Overexpression did not accelerate degeneration beyond controls. *Egr1* modulation in cones of wild-type or *Rho*$^{P23H/+}$ mice did not affect cone survival.

Conclusions: *Egr1* upregulation is a consistent early marker of photoreceptor stress, independent of the nature of the underlying stimulus. Since moderate support for cell survival and preservation of retinal morphology was achieved through the downregulation of *Egr1* expression in rods, but not in cones of the *Rho*$^{P23H/+}$ mouse, the function of EGR1 in degenerative processes may be cell type specific. Although *Egr1* may contribute to disease progression, it is unlikely to be a causative factor for degeneration. Our findings underscore the complexity of the transcriptional response in retinal degeneration and suggest that *Egr1* is a secondary effector of degenerative processes in rods.

Retinitis pigmentosa (RP) is a large heterogeneous group of inherited retinal diseases (IRDs) characterized by a progressive loss of vision. Worldwide, RP affects 1 in 4000 for a total of over 1.5 to 2 million patients having the disease [1,2]. Patients typically first experience the loss of night vision during adolescence, followed by the loss of peripheral vision in young adulthood and, eventually, central vision. This progression is due to primary rod degeneration, subsequently followed by a second wave of degeneration affecting the cones. The large number of genes linked to the disease accounts for the many phenotypic expression of the disease. Since Dryja and colleagues identified the first gene for RP, rhodopsin [3], more than 100 genes have been found to be causative of RP (RetNet). The *Rho*^{P23H} mouse model of retinal degeneration is commonly used for therapeutic studies as it carries the most prevalent mutation in rhodopsin causing RP in patients [4]. Moreover, the model closely recapitulates the features of the human disease, such as outer nuclear layer (ONL) thinning, shortening of rod outer segments, and rod function being affected to a greater extent than cone function [5]. In this model, the rhodopsin gene carries a C>A mutation at codon 23, leading to the replacement of the amino acid proline with histidine in the protein sequence [6]. Because of the mutant codon, the rhodopsin protein is misfolded leading to aberrant glycosylation and a dysfunctional protein, which can be mislocalized causing cell death [6-8].

A common initial reaction of a cell to diverse exogenous or endogenous stimuli is the rapid and transient activation of immediate-early genes (IEGs). IEGs are activated early at the transcription level in response to stimuli, before any new proteins are synthesized [9]. The early growth response-1 (EGR1; also known as NGFI-A, Kro×-24, TIS8, or Zif268) is

Correspondence to: Christian Grimm, Laboratory for Retinal Cell Biology, Department of Ophthalmology, University Hospital Zurich, University of Zurich, Wagistrasse 14, Schlieren, 8952, Zurich, Switzerland: email: cgrimm@opht.uzh.ch

an IEG whose transcription is rapidly induced by a wide array of stimuli, such as growth factors [10], glucose increase [11], hypoxia [12], UV irradiation [13,14], and mechanical stimulation [15]. As a transcription factor, EGR1 is involved in the regulation of many physiologic and pathological processes. In the brain, EGR1 is particularly studied in connection to N-methyl-D-aspartate (NMDA) receptor activation and thought to modulate downstream signaling pathways by adjusting gene expression [16-20]. EGR1 is also readily expressed in the dentate gyrus of the hippocampus where it mediates long-term potentiation, a process essential for both long-term memory storage and memory reconsolidation after retrieval [21]. Beyond the nervous system, EGR1 has often been studied in cancer biology, where it can have contradictory effects acting as both an oncogene [22-25] and a tumor suppressor by regulating genes such as TGF-β1, PTEN, and p53 [26].

In the developing eye and retina, EGR1 has been implicated in numerous pathways regulating ocular growth and neural retina development across different species including chicken, mice and zebrafish [27-31]. In the adult mouse retina, EGR1 expression in the inner retina is both circadian- [32] and light-driven [33-35]. While not expressed in darkness, light onset generates a signal that is transmitted from photoreceptors, with a major contribution of cones [36], to inner retinal neurons rapidly inducing EGR1 expression in various cell types in the inner nuclear layer (INL) and ganglion cell layer (GCL). In pathological contexts, however, EGR1 is upregulated in microglia and/or rods and cones at early phases of degeneration: In retinoschisis mice (*Rs1h*$^{Y/-}$), *Egr1* upregulation preceded the expression of several microglia-related genes, suggesting a possible causative role in the disease [37,38]. Similar results were found in vitro, where lipopolysaccharide-stimulated BV-2 microglia cells strongly upregulated *Egr1* before the expression of microglia-activation markers. However, apoptosis and microglia activation was not prevented by knocking out *Egr1* in *Rs1h*$^{Y/-}$ mice, suggesting that a functional *Egr1* gene is not essential for these processes. Similarly, Sharma and colleagues reported *Egr1* upregulation and microglia activation in the rds mouse model. Since this was observed at a time subsequent to photoreceptor cell death, the authors concluded that photoreceptor apoptosis in this model is at least partially independent of *Egr1* and hypothesized that the activation of the gene might represent a protective immune response [39]. In a more recent publication, *Egr1* positively correlated with photoreceptor cell death in the rd1 mouse [40]. The authors proposed in their ex vivo study that EGR1 controls cell death via regulation of *Parp1* expression, a gene that was previously implicated in the degenerative processes in several RP animal models [41-43]. Lastly, in a droplet-based single-cell RNA sequencing study of rd10 mice, a pseudotime analysis of the transcriptome of individual rod cells showed that *Egr1* was one of the most highly upregulated transcripts in the early phase of degeneration [44]. Its upregulation, however, was transient, with rods ceasing to express *Egr1* in the later phase of cell death. The upregulation of *Egr1* was also detected in cones that, however, continued to express *Egr1* as degeneration progressed [44]. These studies suggest that the early activation of EGR1 is a unifying feature across a variety of genetically heterogeneous models of retinal degeneration. However, conclusive in vivo data are still missing to understand the role of EGR1 in photoreceptor cell death.

In this study, we used *Rho*$^{P23H/+}$ mice to investigate the effects of the cell type-specific modulation of *Egr1* in retinal degeneration. Because of their rather slowly progressing degeneration [6], the *Rho*$^{P23H/+}$ mice offer a large time window for genetic manipulations that aim to protect photoreceptors. To modulate *Egr1* expression specifically in rods or cones, we used AAV-mediated RNA interference (RNAi) and gene overexpression and analyzed the consequences of decreased or increased *Egr1* expression in wt and *Rho*$^{P23H/+}$ mice over time. To overcome known disadvantages of conventional small interfering RNAs (siRNAs) [45], we adopted the microRNA-based shRNAmir system [46]. This system channels the cargo RNA into the endogenous miRNA processing pathway at the level of DROSHA in the nucleus [47,48], ensuring precise siRNA cleavage while minimally interfering with the natural microRNA processing machinery [48]. Cell-type specificity was achieved by using a combination of AAV capsid variants [49,50] and gene promoters [51,52] to target specifically either rods or cones.

METHODS

Animals: Animal experimentation was approved by the Cantonal Veterinary Office of Zürich, Switzerland (license numbers: ZH019/2019 and ZH105/2022) and adhered to the ARVO statement for the use of Animals in Ophthalmic and Vision Research. Wild-type (C57BL6/J, 129S6*)* and transgenic mice (*Rho*$^{P23H/P23H}$, *Rho*$^{P23H/+}$) were housed at the Laboratory Animal Services Centre (LASC) of the University of Zürich with a 14/10 h light/dark cycle and an average light intensity of 60–150 lx at cage level. *Rho*$^{P23H/P23H}$ mice (strain # 017,628, Jackson laboratory, Bar Harbor, ME) were bred with C57BL6/J wild-type mice to generate *Rho*$^{P23H/+}$ mice. All mice used were tested negative for the rd8 mutation in the Crumbs 1 (*Crb1*) gene [53,54].

Lentiviral-mediated generation of shEgr1 expressing stable cell lines, PMA treatment, and transgenic Egr1

overexpression in 661W: The photoreceptor-derived 661W cell line [55] and HEK293T (ATCC CRL-3216) cells were cultured in DMEM, 10% heat-inactivated FBS (Gibco, Thermo Fisher Scientific, Waltham, MA) and 1% penicillin-streptomycin (Gibco, Thermo Fisher Scientific) at 37 °C and 5% CO_2. For gene silencing, lentiviral-pseudotyped particles were used to generate stable cell lines expressing shRNAs against *Egr1* (Sigma-Aldrich, St. Louis, MO; Table 1) and a non-targeting scrambled shRNA (SHC002, Sigma-Aldrich; Table 1). To prepare lentiviral particles, HEK293T cells were cultured in 75 cm^2 flasks and co-transfected with shRNAs in combination with the ViraPower lentiviral expression vector system and Lipofectamin 3000 (Invitrogen, Thermo Fisher Scientific) in serum-free medium. The serum-free medium was replaced the next day with complete medium. The culture supernatants containing the lentivirus particles were collected 48–72 h post-transfection, cleared by centrifugation at 200 g for 5 min, and filtered through a 0.45 µm pore size filter (Merck & Co., Schaffhausen, Switzerland). Filtrates were applied in a 1:1 mixture with medium containing 6 µg/ml polybrene (Sigma-Aldrich) to infect 661W cells. Infected cells were selected with 2 µg/ml puromycin for 2–3 weeks. To induce endogenous expression of *Egr1*, cells were treated with 10 ng/mL of phorbol 12-myristate 13-acetate (PMA, P1585-P1MG, Sigma-Aldrich) in DMSO (D8418, Sigma-Aldrich) for 1 h. Subsequently, cells were washed once with 1X PBS (Gibco), harvested, and RNA prepared for real-time PCR to investigate gene expression (see below).

To overexpress *Egr1*, 661W cells were seeded at a density of 50’000 cells/ml in wells of 12-well plates and incubated overnight. Cells were transfected with Lipofectamine 3000 (Invitrogen, Thermo Fischer Scientific) and 1 µg of plasmid DNA containing the overexpression or a control plasmid (see next section) in Opti-MEM (Thermo Fischer Scientific) for 24 or 48 h. Subsequently, cells were washed once with 1X PBS (Gibco), harvested, and RNA was prepared for real-time PCR (see below).

Plasmid cloning and AAV generation: shRNAmir DNA fragments containing *shEgr1* or *shCtrl* sequences were designed using the miR-E backbone following the recommendations by Fellmann [46] and synthesized by Genewiz (Azenta Life Science, South Plainfield, NJ). The shRNA cassettes were cloned in the 3′UTR of GFP. For overexpression, the *Egr1* coding sequence from mouse (*mEgr1*; Addgene plasmid #11729) [56] was connected with a P2A cassette to a GFP coding sequence and cloned downstream of the ubiquitous cytomegalovirus (CMV) promoter in an AAV2 backbone for in vitro experiments (AAV2::CMV-mEgr1-P2A-eGFP-pA-WPRE). A pcDNA3-CMV-eGFP plasmid (Clontech, Addgene #2487) was used as control. To achieve cell specificity in vivo, constructs were placed under control of the mOP (mouse opsin) promoter [52] to transduce rods, and an engineered human OPN1WM (opsin medium wavelength) promoter to target middle wavelength (M) cones [51]. All constructs were cloned into an AAV backbone with mutated type 2 inverted terminal repeats (ITRs), and packaged into the AAV2(QuadYF+TV; 7m8)/2 capsid variant containing five point mutations (Y272F, Y444F, T491V, Y500F, and Y730F) [49] to target rods, and into the AAV2/7m8 capsid [50] to target cones. Due to AAV packaging limitations, the cone-specific overexpression vector did not contain eGFP.

Subretinal injections: Injections were performed at 4 weeks of age as described earlier [57]. Briefly, pupils were dilated with 1% cyclogyl (Alcon Pharmaceuticals, Fribourg, Switzerland) and 5% neosynephrin (Ursapharm Schweiz GmbH, Hünenberg, Switzerland). Mice were anesthetized with a subcutaneous injection of ketamin (85 mg/kg, Pfizer AG, Zürich, Switzerland) / xylazine (10 mg/kg, Elanco Animal Health GmbH, Basel, Switzerland) and placed on a heating pad set to 37 °C during the procedure. Lacrinorm® Carbomerum (Bausch & Laumb Swiss AG, Zug, Switzerland) was applied to keep the eyes moist. The head was held by a stereotactic adaptor (Hugo Sachs Elektronik – Harvard Apparatus GmbH, March–Hugstetten, Germany) and the temporal sclera was punctured with a 30G needle beneath the ora serrata. A

Table 1. *Egr1*-targeting and control shRNA sequences.

Name	Sigma-Aldrich clone ID	Insert sequence	Target region on *Egr1*	Affinity to *EGR1*
Sequence 1	TRCN0000231218	GGATGAGCTTACCCGCCATAT	CDS	0 mismatches
Sequence 2	TRCN0000374054	GATAATTTGCATACTCTATTG	3′UTR	1 mismatch
Sequence 3	TRCN0000081627	GCTCTTAATACCACCTACCAA	CDS	4 mismatches
Sequence 4	TRCN0000231216	CACTCCACTATCCACTATTAA	CDS	5 mismatches
Sequence 5	TRCN0000374131	GACTTGATTTGCATGGTATTG	3′UTR	4 mismatches
Sequence 6	TRCN0000231219	GACCATCAAGTTGGCATAAAG	3′UTR	5 mismatches
Ctrl sequence	SHC002	CAACAAGATGAAGAGCACCAA	NA	NA

5 µl Hamilton syringe with a 34G blunt-end needle (Hamilton Bonaduz AG, Bonaduz, Switzerland) was placed in a micromanipulator (H. Saur Laborbedarf, Reutligen, Germany) and inserted through the pre-punctured site for the transvitreal subretinal injection of 1 µl AAV solution nasally to the optic nerve. All AAVs were applied at a concentration of 1×10^9 vg/µL. To visually control the procedure, the injection solution was supplemented with 10% fluorescein (1 mg/ml, Akorn Inc., IL). After injections, 1 drop of viscotears (Bausch+Lomb, Vaughan, Canada) was applied, and anesthesia was reversed with atipazemole (2 mg/kg, Graeub, Bern, Switzerland). Mice were placed on a heating pad until fully awake. Two to three weeks after injection, mice were subjected to fluorescent funduscopy and optical coherence tomography (OCT) to test for transgene expression and to detect potential injection-inflicted tissue damages, such as bleeding or persistent retinal detachment. Such eyes were excluded from the study.

White light damage: To induce retinal degeneration, mice were exposed to high levels of white light as described in [58]. Briefly, 129S6 mice were placed in darkness the evening before the experiment. Thirty min before light exposure, pupils were dilated (as described above) in dim red light. The mice were placed in cages without a grid but lined with aluminum foil (to homogeneously distribute light within the cage), which were positioned under the light-exposure device to reach 13'000 lx at cage level. Exposure lasted for 1 h. After this time, mice were returned to their home cages and kept in darkness for 24 h. Afterwards, mice were housed in the normal light/dark cycle until analysis.

In vivo imaging by funduscopy and optical coherence tomography: Anesthesia and pupil dilation were performed as described above. One drop of 2% methocel (OmniVision AG, Neuhausen, Switzerland) was applied to keep the eyes moist. Fundus images and OCT scans were acquired using the Micron IV system (Phoenix Research Labs, Pleasanton, CA) equipped with filters for imaging green fluorescence.

RNA isolation and real-time PCR: Mice were euthanized with CO_2 inhalation followed by decapitation. Retinas were isolated through a slit in the cornea and snap-frozen in liquid nitrogen. To separate the transduced from the untransduced retinal area, the retina was flattened out and cut in half using the GFP signal as guidance. The two halves were snap-frozen in liquid nitrogen. RNA from tissue or cells was isolated using an RNA isolation kit (NucleoSpin RNA, Macherey-Nagel GmbH & co.KG, Düren, Germany) according to the manufacturer's instructions, including an on-column DNase digestion step (740,963, Macherey-Nagel GmbH & co.KG). First-strand cDNA synthesis was performed using M-MLV reverse transcriptase (Promega, Dübendorf, Switzerland), 650 ng of total RNA and 20 pmol of oligo-dT primers. Gene expression was analyzed via semiquantitative real-time PCR (QuantStudio 3, Thermo Fisher Scientific) using 10 ng of cDNA template and PowerUp SYBR green Master Mix (Thermo Fisher Scientific). Primer pairs for *Egr1* (F: 5′-ACA ACC CTA TGA GCA CCT GAC C-3′; R: 5′-GGC AGA GGA AGA CGA TGA AG-3′), *Actb* (F: 5′-CAA CGG CTC CGG CAT GTG C-3′; R: 5′-CTC TTG CTC TGG GCC TCG-3′), and *Atf3* (F: 5′-ACC TCC TGG GTC ACT GGT ATT TG-3′; R: 5′-TTC TTT CTC GCC GCC TCC TTT TCC-3′) were designed to span large intronic regions and avoid known single nucleotide polymorphisms in the mouse sequence. Normalization was performed with *Actb* as housekeeping gene, and relative expression was calculated using the comparative threshold cycle method ($2^{-\Delta\Delta CT}$) [59].

Determination of ONL thickness and immunofluorescence: To determine the thickness of the ONL, dorsally marked eyes were enucleated and fixed in 2.5% glutaraldehyde at 4 °C overnight. Dissected eyes were post-fixed in 1% osmium tetroxide for 1 h and embedded in Epon812 (Sigma-Aldrich). Nasal-temporal sections (0.5 µm) were cut through the optic nerve head, counterstained with toluidine blue, and analyzed by light microscopy (AxioImager Z2, Carl Zeiss AG, Feldbach, Switzerland). Retinal panoramas were reconstructed from single 10X images using Adobe Photoshop CS6 (Adobe Systems, Inc.). The ONL thickness (from the outer limiting membrane to the outer plexiform layer) was measured every 200 µm starting from the optic nerve head with the Adobe Photoshop CS6 ruler tool.

Eyes for immunofluorescence analysis were marked and fixed in 4% PFA in 0.1 M PBS for 1.5 h at 4 °C. After removal of the lens, eyes were cryo-protected in 30% sucrose (Sigma-Aldrich) in 0.1 M PBS for at least 2 h, embedded and frozen in freezing medium (O.C.T., Leica Biosystems, Nussloch, Germany). Embedded eyes were stored at −80 °C until cut into 12 µm thin sections. Immunolabelling was performed overnight at 4 °C with the following primary antibodies: anti-EGR1 (1:500, MA5–15008, Thermo Fisher Scientific), anti-RHO (1:100, O4886, Sigma-Aldrich), anti-OPN1SW (1:500, sc-14363, Santa Cruz, Dallas, TX) and anti-ARR3 (AB15282, 1:1000, Merck & Co.). Peanut Agglutinin (PNA) lectin from *Arachis hypogaea* (peanut) conjugated with Alexa Fluor™ 647 (L32460, Thermo Fischer Scientific) was used to label the cone interphotoreceptor matrix [60]. Incubation of primary antibodies and PNA was done in blocking solution containing 3% normal goat serum (Sigma-Aldrich) and 1% Triton X-100 (Sigma-Aldrich) in PBS. The next day, sections were washed, incubated with the appropriate secondary antibodies in

blocking solution for 1 h, and with 4',6-diamidino-2-phenylindole (DAPI, 1:6000) in 0.1 M PBS for 3 min. Sections were mounted with MOWIOL (Sigma-Aldrich) antifade medium and imaged using a fluorescence microscope (AxioImager Z2, Carl Zeiss AG). To count cone cells, retinal panoramas from immunofluorescence images were reconstructed with Adobe Photoshop CS6, and 600 µm-wide sections were selected within the transduced and the untransduced areas of the same retina. Cones (ARR3-positive cells) were counted in these areas using the multi-point tool in ImageJ (Version 1.52a).

Statistical analysis: Statistical analysis was performed using GraphPad Prism (GraphPad Software, San Diego, CA). Significance was tested by an unpaired *t* test when two independent groups were compared, or a paired *t* test when the two measurements came from the same animal. When more than 2 groups were compared, a one-way ANOVA followed by a Tukey's (when all groups were compared to each other) or Dunnett's (when all groups were compared to a specific group) multiple comparison test was applied. When assessing the influence of two independent variables and their interaction (2×2 factorial design), a two-way ANOVA was applied. Data were considered significantly different with $p \leq 0.05$. Only p values <0.05 are shown in the figures. All tests and number of animals/samples are indicated in the figure legends.

RESULTS

In wild-type mice, EGR1 expression is largely restricted to several cell types of the inner retina and can follow both circadian [32] and diurnal inputs [33,35] and is, at least partially, driven by light-induced signaling from cones [36]. However, in the presence of noxious stimuli, photoreceptors upregulate EGR1 expression early during degeneration [44]. Despite the vast genetic and phenotypic heterogeneity of retinal diseases, the upregulation of EGR1 in the ONL is a common feature across many degenerative mouse models, such as the rd10 [44], the rd1 [40], and the *Rsh1*$^{-/Y}$ [37,38] mice. To investigate the potential of reducing or increasing *Egr1* expression in photoreceptors as an approach to protect the retina, we employed the *Rho*$^{P23H/+}$ mouse, a slowly degenerating RP model offering a large treatment window [6]. Similar to other models, EGR1 was expressed in photoreceptors of *Rho*$^{P23H/+}$ mice at different stages of degeneration (8, 12, 16 weeks of age), in contrast to age-matched wild-type mice that did not express EGR1 in their outer retina (Figure 1A). Interestingly, expression of EGR1 in the inner retina appeared less prominent in *Rho*$^{P23H/+}$ than in wild-type mice. The reason for this is unknown but may involve disturbed signaling from damaged photoreceptors. Since *Egr1* expression in rods was shown to be only transiently induced during the early phase of cell death [44], only a fraction of cells is positive for EGR1 at any given time point, especially in a slowly degenerating retina. This fraction may be higher in models of induced, synchronized cell death, such as the light damage model. Indeed, damaging levels of light caused *Egr1* expression to rapidly increase in the retina 2 h after exposure. The transient nature of *Egr1* induction is clearly demonstrated by the rapid decline in expression levels at 6 h after exposure, reaching nearly basal levels after 24 and 48 h (Figure 1B). As expected, not all rods and cones were positive for EGR1 in the *Rho*$^{P23H/+}$ retina at 8 weeks of age due to the transient nature of EGR1 induction in the degenerating retina (Figure 1C, D).

Collectively, these data show that *Egr1* is induced also in photoreceptors of the *Rho*$^{P23H/+}$ mouse and the retina after exposure to damaging light intensities. This further strengthens the hypothesis that EGR1 expression in the ONL is a common characteristic of retinal degeneration, regardless of the underlying mutation or insult. To approach the functional significance of this upregulation, we modulated *Egr1* expression in rods and cones of the *Rho*$^{P23H/+}$ mouse in vivo.

Targeting Egr1 for knockdown and transgenic overexpression: To modulate *Egr1* expression in vivo, we chose shRNA-based RNA interference (RNAi) and transgenic overexpression methods to decrease or increase endogenous EGR1 levels, respectively. To identify an effective sequence for RNAi, we generated six 661W cell lines that stably expressed different *Egr1* shRNAs (Table 1) and determined endogenous *Egr1* mRNA levels by real-time PCR. Five out of the six shRNA sequences significantly reduced *Egr1* mRNA levels in the cell lines, with sequence 1 being the most effective (78% downregulation; Figure 2A). This cell line was selected for investigating shRNA-mediated *Egr1* silencing also under stress conditions. For this purpose, control 661W and 661W-*shEgr1* cells were treated with 10 ng/mL PMA, a well known *Egr1* activator via the stress-activated MAPK pathways [61], for 1 h and tested for endogenous *Egr1* mRNA expression. PMA increased *Egr1* levels 3.8-fold in both control and 661W-*shEgr1* cells. Importantly, *Egr1* levels after PMA treatment were 55% lower in 661W-*shEgr1* cells than in control cells (Figure 2B), demonstrating that the shRNA repressed endogenous *Egr1* also in stressed cells, which is essential for using this approach in degenerating photoreceptors. Transfection of 661W cells with the overexpression plasmid resulted in a 22.6- and 15.6-fold increase in *Egr1* mRNA levels at 24 and 48 h post-transfection, respectively (Figure 2C). The overexpression resulted in functional EGR1 proteins, as evidenced by the 13.6-fold upregulation of the EGR1 target gene *Atf3*

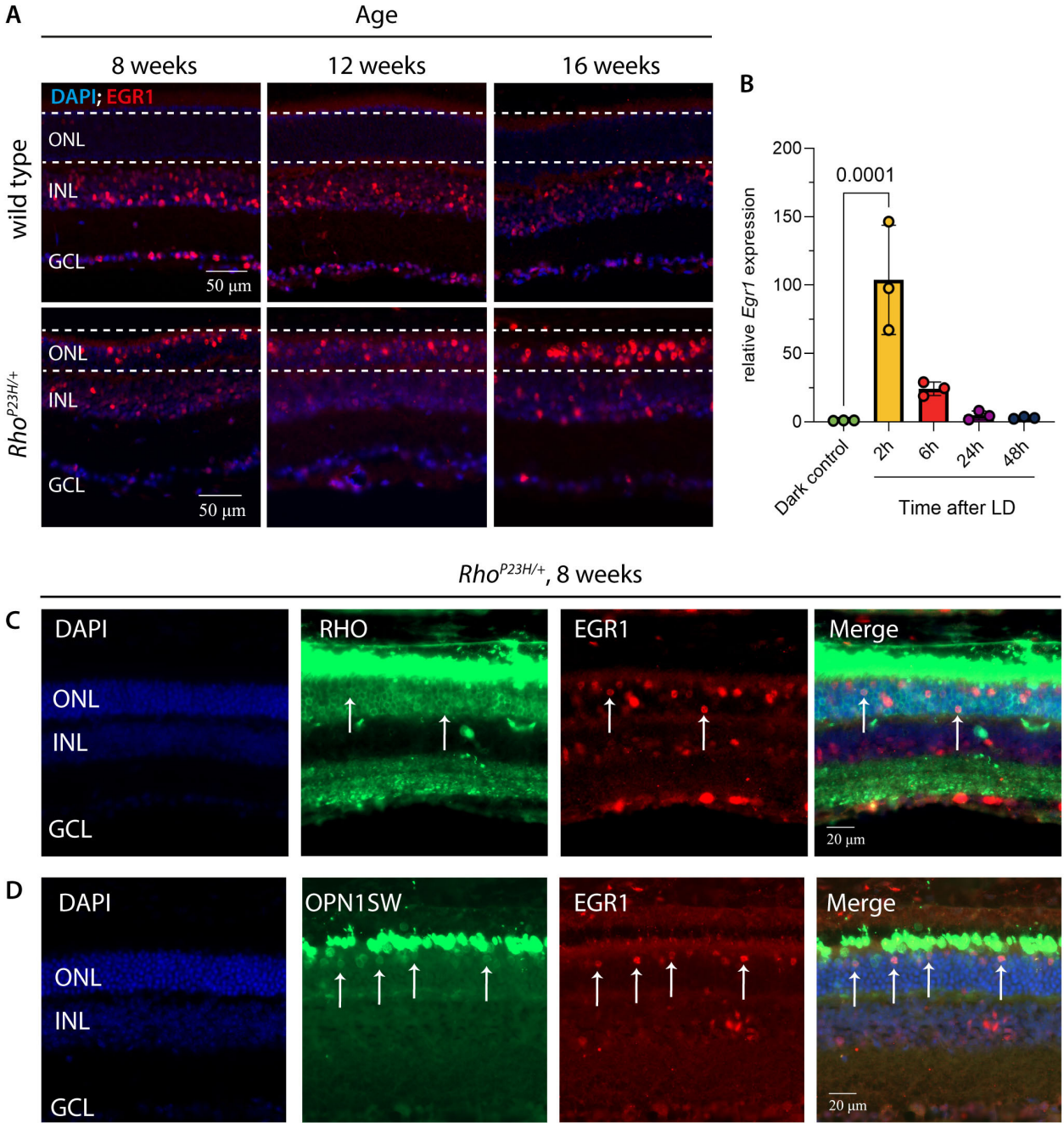

Figure 1. EGR1 expression in *Rho*$^{P23H/+}$ mice and after light damage. **A**: Immunofluorescence staining of EGR1 (red) in retinal sections from 8, 12, 16-week-old wild-type and *Rho*$^{P23H/+}$ mice. DAPI (blue) was used to visualize cell nuclei. Scale bar: 50 µm. **B**: Real-time qPCR of retinal *Egr1* expression in the model of light-induced degeneration. Levels are expressed relative to non-exposed dark controls (ctrl), which were set to 1. Shown are individual data points and means ± SD n=3. One-way ANOVA with Dunnett's multiple comparisons test, p value as indicated. **C**, **D**: Immunofluorescence staining of retinal sections from 8-week-old *Rho*$^{P23H/+}$ mice for RHO and EGR1 (**C**) and OPN1SW and EGR1 (**D**), showing EGR1 expression in degenerating rods and cones. White arrows point to RHO (C) or OPN1SW (D) positive cells expressing EGR1. Scale bar: 20 µm. ONL: outer nuclear layer; INL: inner nuclear layer; GCL: ganglion cell layer; LD: light damage.

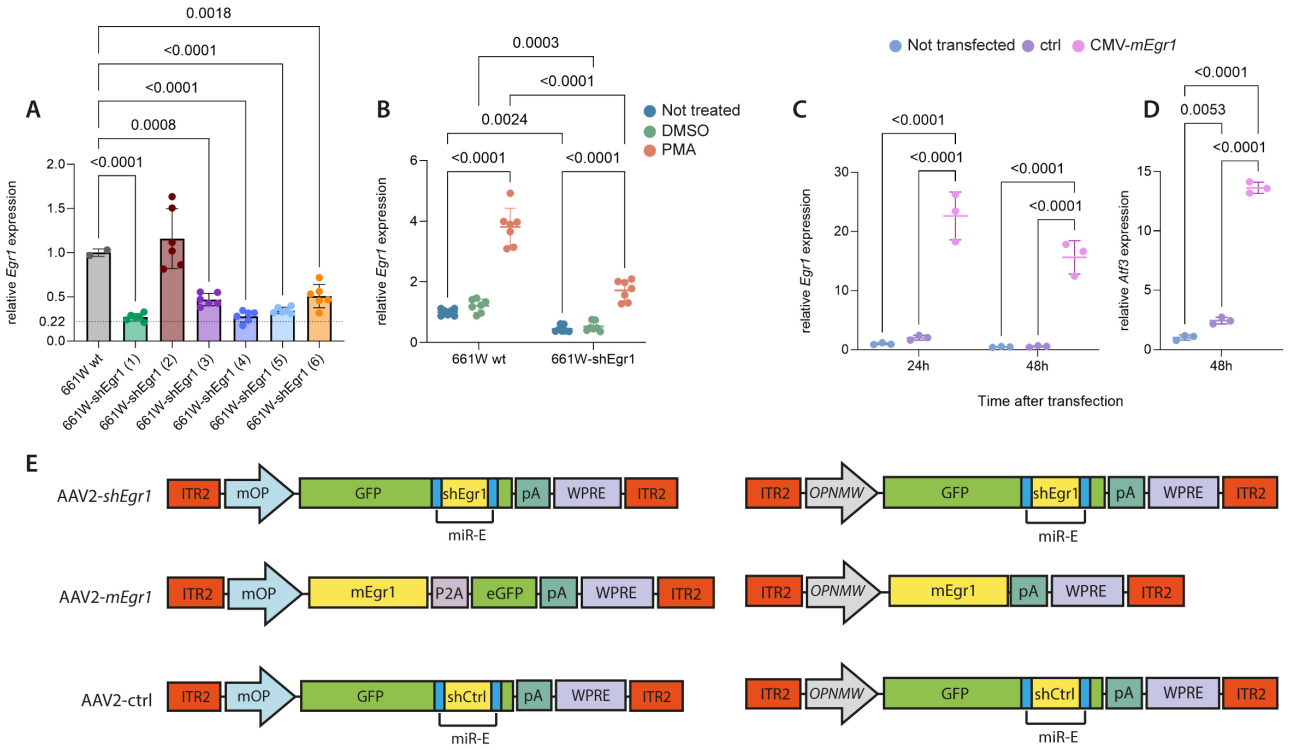

Figure 2. In vitro validation of *shEgr1* and *mEgr1* sequences and design of AAV vectors. **A**: Real time PCR for *Egr1* in 661W cell lines stably expressing shEgr1. Each cell line (plotted on the x-axis) expresses a different *shEgr1* sequence (1–6, Table 1). Sequence (1) showed the strongest downregulation (78%, dotted line) and was chosen for further tests. Shown are individual data points and means ± SD n=6. One-way ANOVA with Dunnett's multiple comparisons test, p values as indicated. **B**: PMA stress test in 661W wt and 661W-shEgr1 (1) cells. Shown are individual data points and means ± SD n=7. Two-way ANOVA with Dunnett's multiple comparisons test, p values as indicated. **C**: In vitro test of the *Egr1* overexpression plasmid AAV2::CMV-mEgr1-P2A-eGFP-pA-WPRE (CMV-mEgr1) in 661W cells. *Egr1* mRNA levels were determined at 24 h and 48 h after transfection of the overexpressing plasmid (pink) and compared to cells that were not transfected (blue) and cells that received the pcDNA3-CMV-eGFP control plasmid (purple). Shown are individual data points and means ± SD n=3. One-way ANOVA with Tukey's multiple comparisons test, p values as indicated. **D**: Expression levels of the EGR1 target gene *Atf3* in untransfected (blue), ctrl-transfected (purple) and CMV-mEgr1-transfected (pink) cells at 48 h after transfection. Shown are individual data points and means ± SD n=3. One-way ANOVA with Tukey's multiple comparisons test, p values as indicated. **E**: Schematic representations of the *Egr1* downregulation (AAV2-*shEgr1*, top), *Egr1* overexpression (AAV2-*mEgr1*, middle), and control (AAV2-ctrl, bottom) AAV vectors. ITR2: inverted terminal repeats of serotype 2; mOP: mouse opsin promoter (rod-specific); *OPN1MW*: human opsin medium wavelength promoter (cone-specific); (e)GFP: (enhanced) green fluorescent protein; pA: poly-A tail; WPRE: woodchuck hepatitis virus posttranscriptional regulatory element; miR-E: microRNA-E backbone for shRNAs; P2A: 2A self-cleaving peptide.

(activating transcription factor 3 [62,63]) 48 h after transfection (Figure 2D). The small induction of *Atf3* expression in control-transfected cells may have been caused by a slight stress induced by the serum-reduced OptiMEM transfection medium [64].

To generate AAVs for the in vivo experiments, we cloned the sequence for knocking down *Egr1* (*shEgr1*) and the control sequence (*shCtrl*, Table 1) into the miR-E scaffold [46] and placed the cassettes in the 3′-untranslated region (UTR) of GFP (Figure 2E). The AAV construct for overexpression contained the mouse *Egr1* (*mEgr1*) coding sequence connected to eGFP via a P2A site. All constructs were cloned downstream of the rod-specific (mOP [52]) and the cone-specific (*OPN1MW* [51]) promoter. Due to the limited AAV packaging capacity, the cone-specific overexpression construct did not contain eGFP (Figure 2E, Table 2).

Modulation of Egr1 expression in rods of wild-type mice: To assess the potential of our constructs to modulate *Egr1* expression in rods, we injected the AAVs carrying the *shEgr1*, the *mEgr1* or the control sequence under control of the mOP promoter into the subretinal space of 4-week-old wt mice and assessed their transduction and expression profiles. At 8 weeks post-injection (wpi, 12 weeks of age), the injection sites were visible as hyperreflective spots in the fundus images (Figure 3A-C, arrows) and minor disturbances to the retinal layering in OCT scans (blue lines and frames). However, OCT

Table 2. AAV constructs.

Name	Cell targeted	Capsid	Construct
mOP-mEgr1	Rods	AAV2(QuadYF+TV; 7m8)/2	mOP-mEgr1-P2A-eGFP-WPRE
mOP-shEgr1	Rods	AAV2(QuadYF+TV; 7m8)/2	mOP-GFP-shEgr1-WPRE
mOP-ctrl	Rods	AAV2(QuadYF+TV; 7m8)/2	mOP-GFP-shCtrl-WPRE
***OPN1MW*-mEgr1**	Cones	AAV2/7m8	*OPN1MW* -mEgr1-WPRE
***OPN1MW*-shEgr1**	Cones	AAV2/7m8	*OPN1MW* -GFP-shEgr1-WPRE
***OPN1MW*-ctrl**	Cones	AAV2/7m8	*OPN1MW* -GFP-shCtrl-WPRE

All AAVs have type 2 ITRs, one wild-type and one mutated. mOP: mouse opsin promoter; *OPN1MW*: opsin medium wavelength promoter; (e)GFP: (enhanced) green fluorescent protein; P2A: 2A self-cleaving peptide; WPRE: woodchuck hepatitis virus posttranscriptional regulatory element.

scans through the optic nerve head (red lines and frames) demonstrated that the retinal layers were overall preserved, excluding toxicity of the vectors or the transgenic sequences in normal retinas. Fluorescent funduscopy indicated that approximately 20%–30% of the retinal area was transduced. Immunostaining of retinal sections for rhodopsin (RHO) and imaging of (e)GFP fluorescence (surrogate marker for AAVs) showed that transgene expression was restricted to photoreceptors (Figure 3A-C, lower panels). Since EGR1 is activated upon damage or stress [40,44], it is important to note that injections did not cause widespread EGR1 expression *per se,* as only few rods transduced with AAV::mOP-ctrl (Figure 3A) co-expressed endogenous EGR1 and GFP. Similarly, only very few EGR1-positive photoreceptor nuclei were detected after injection of AAV::mOP-*shEgr1* (Figure 3B). Whether this was due to an efficient downregulation of *Egr1* expression by the shRNA or to the absence of stress after the injection, as suggested by the control virus, could not be determined. In contrast, injection of AAV::mOP-*mEgr1* resulted in a large number of EGR1-positive cells in the ONL, indicating a strong transgenic expression of *Egr1* in rods (Figure 3C). To assess the strength of the overexpression, we used real-time PCR to amplify *Egr1* from total retinal RNA isolated from dark-adapted mice two weeks after injection. Even though we used total retinal RNA that was isolated not only from the 20%–30% transduced rods but also from all non-transduced cells in the outer and inner retina, we detected a significant increase in *Egr1* expression in retinas injected with AAV::mOP-*mEgr1* (Figure 3D). Due to the presence of RNA from untransduced cells in the analysis, the measured twofold increase underestimates the strength of upregulation in transduced cells. Since *Egr1* is not, or only very weakly, expressed in healthy rods, we could not evaluate the in vivo efficacy of our *shEgr1* sequence in wild-type mice. Therefore, we assessed retinal *Egr1* levels in *Rho*$^{P23H/+}$ mice at 12 wpi (16 weeks of age). To increase the specificity of our analysis, we separated the untransduced and transduced halves of the retina using the GFP signal as guidance, then isolated total RNA from each half separately. While *Egr1* mRNA levels in the retinas of control-injected mice did not differ between the untransduced and transduced areas, *Egr1* was significantly downregulated after injection of AAV::mOP-*shEgr1* (Figure 3E). Lastly, we measured the ONL thickness in wild-type mice at 8 wpi to directly address potential retinal toxicity of our AAVs (Figure 3F). The similar ONL thickness between treatments indicated that modulation of *Egr1* expression in healthy rods did not cause cellular toxicity. Although significant, the slight increase in ONL thickness (approximately 3 µm) in AAV::mOP-*mEgr1* injected mice suggests a minor swelling of the ONL for unknown reasons.

These results demonstrated an effective and specific transduction of rod photoreceptors by the mOP-driven transgenes after AAV-mediated delivery, as shown before [65]. The constructs were able to successfully modify *Egr1* expression, with no adverse effects in wt mice.

Egr1 downregulation delays rod degeneration in Rho$^{P23H/+}$ *mice:* To analyze if the rod-specific modulation of *Egr1* expression affects photoreceptor degeneration we injected the three viruses into the retina of 4-week-old *Rho*$^{P23H/+}$ mice. Immunofluorescence of retinal cross sections at 12 wpi showed that the degenerating retina expressed the transgenes specifically in the ONL (Figure 4A), similarly to the observation made in wt retinas (Figure 3A-C). Since GFP-positive cells only rarely co-localized with EGR1 in AAV::mOP-*shEgr1* injected mice, downregulation of EGR1 in transduced rods of *Rho*$^{P23H/+}$ mice may have been effective. In AAV::mOP-*mEgr1* injected retinas, however, GFP and EGR1 showed strong co-localization indicating upregulation of EGR1 (Figure 4A). While fundus imaging and OCT scans did not show obvious differences between the treatments (Figure 4B), we measured the ONL thickness on retinal cross sections at 4, 8 and 12 wpi (Figure 4C). At 4 wpi, the ONL in mice injected with AAV::mOP-*mEgr1* was slightly

thicker, reflecting the observation already made in wt mice (Figure 3F), while AAV::mOP-*shEgr1* was without effect on the ONL thickness. By 8 wpi, the ONL thickness decreased as degeneration progressed in controls and AAV::mOP-*mEgr1* but not in AAV::mOP-*shEgr1* injected mice. In these latter mice, the ONL thickness was comparable to the thickness at 4 wpi suggesting a protective effect and attenuation of the degeneration by the downregulation of *Egr1* in *Rho*$^{P23H/+}$ rods by RNAi. Interestingly, the overexpression of EGR1 did not accelerate the degenerative process. At 12 wpi, the preservation of rods by the interference with *Egr1* expression was still evident, as the ONL of AAV::mOP-*shEgr1* injected mice was still significantly thicker than the ONL in the controls. The attenuation of degeneration by the AAV::mOP-*shEgr1* injections was also evident by the longitudinal ONL analysis of the different treatments. In contrast to the control and AAV::mOP-*mEgr1* injected mice, thinning of the ONL was not significant in AAV::mOP-*shEgr1* treated mice (Figure 4D). Altogether, these results suggest that *Egr1* moderately contributes to rod degeneration in *Rho*$^{P23H/+}$ mice and that reducing *Egr1* expression delays but does not prevent photoreceptor loss.

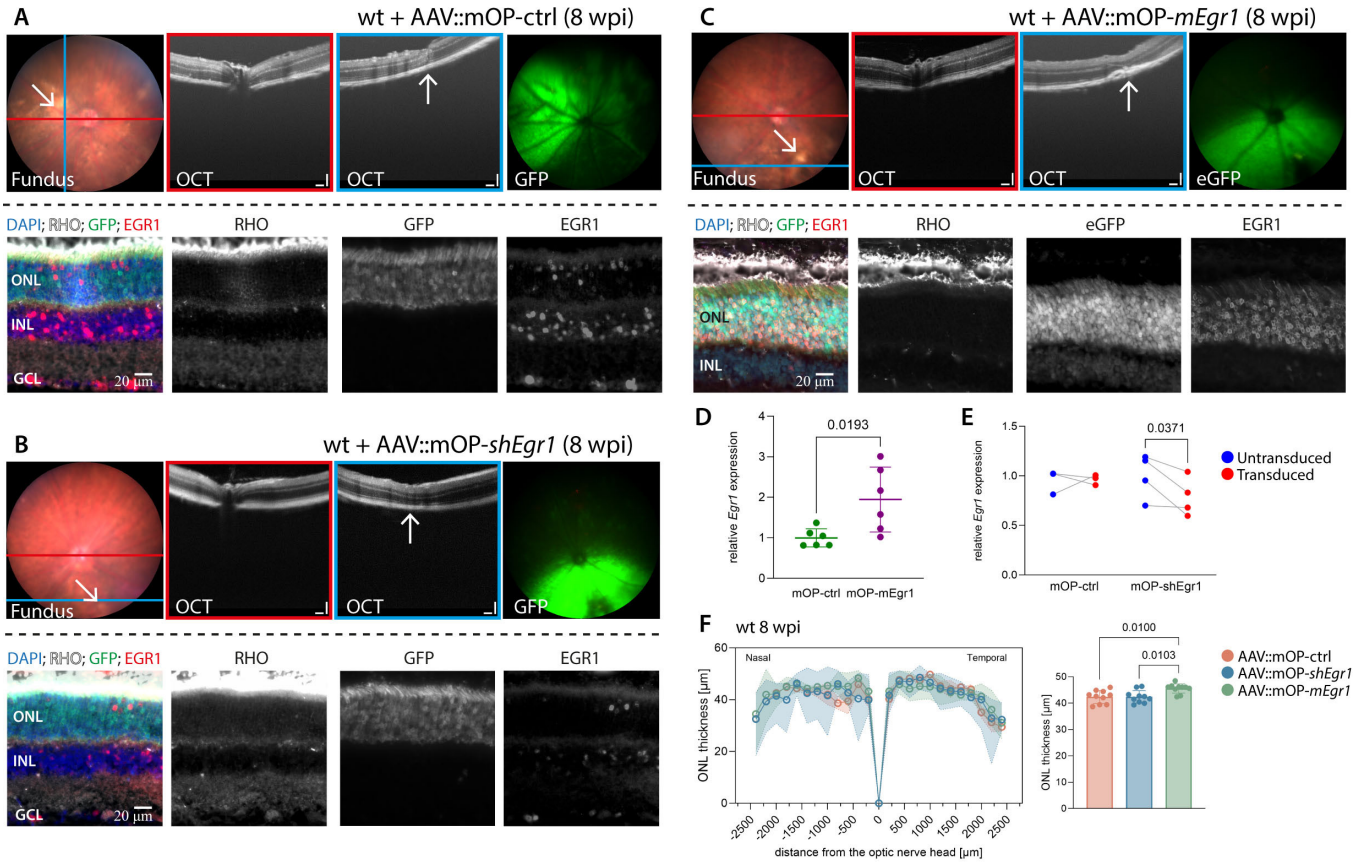

Figure 3. Expression and safety of *shEgr1* and *mEgr1* transgenic elements in wt rods. **A**-**C**: Fundus images and OCT scans (top rows) and immunofluorescence images (bottom rows) of wt retinas subretinally injected with (**A**) AAV::mOP-ctrl, (**B**) AAV::mOP-sh*Egr1* and (**C**) AAV::mOP-*mEgr1* at 8 wpi. White arrows point to injection sites. OCT scans are color-coded in red when across the optic nerve, or blue when across the injection site. Immunofluorescence panels show the transduction pattern of the virus (GFP), individual EGR1 and rhodopsin (RHO) signals as gray-scale images and the colored merge. Scale bars: 20 µm. **D**: *Egr1* mRNA levels in retinas of wt mice injected with mOP-ctrl (green) or mOP-*mEgr1* (purple) at 2 wpi. Shown are individual data points and means ± SD n=6. Unpaired one-tailed *t* test, p value as indicated. **E**: *Egr1* mRNA levels in transduced (red) and untransduced (blue) retinal areas of *Rho*$^{P23H/+}$ mice injected with mOP-ctrl or mOP-*shEgr1* at 12 wpi. Corresponding retinal areas of the same eye are connected by lines. n=3–4. Paired one-tailed *t* test, p value for mOP-ctrl: 0.4567, p value for mOP-shEgr1 as indicated. **F**: Left: spidergrams showing the mean and range of the ONL thickness of wt mice injected with mOP-ctrl, mOP-*shEgr1* or mOP-*mEgr1* at 8 wpi. Measurements were taken every 200 µm from the optic nerve head (0 µm). Right: quantification of the ONL thickness of the nasal (transduced) retina after AAV injections. Each dot represents the average thickness at a particular distance (every 200 µm from 400 µm to 2200 µm) from the optic nerve head. Shown are means ± SD. One-way ANOVA with Tukey's multiple comparisons test, p values as indicated. n=5–7. ONL: outer nuclear layer; INL: inner nuclear layer; GCL: ganglion cell layer.

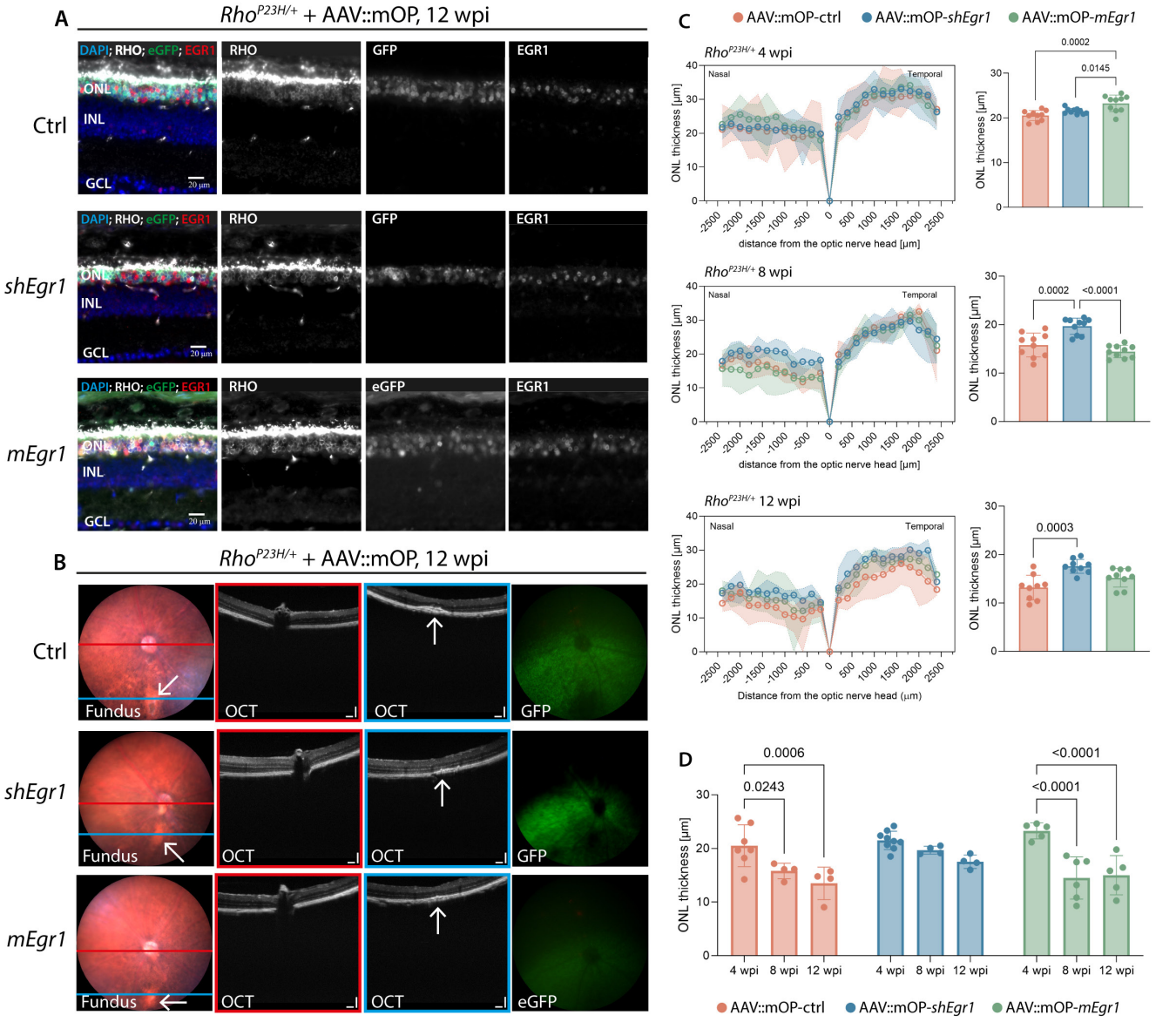

Figure 4. Phenotypic evaluation of mOP-driven AAVs in *Rho*$^{P23H/+}$ mice. **A**: Immunofluorescence images of *Rho*$^{P23H/+}$ retinas injected with AAV::mOP-ctrl (Ctrl), AAV::mOP-*shEgr1* (*shEgr1*), and AAV::mOP-*mEgr1* (*mEgr1*) at 12 wpi. Individual panels show the transduction pattern of the virus (GFP) as well as EGR1 and rhodopsin (RHO) positive cells as grayscale images and the colored merge. Scale bars: 20 µm. (**B**) Fundus images and OCT scans of *Rho*$^{P23H/+}$ retinas injected with AAV::mOP-ctrl (Ctrl), AAV::mOP-*shEgr1* (*shEgr1*), and AAV::mOP-*mEgr1* (*mEgr1*) at 12 wpi. White arrows point to injection sites; OCT scans are color-coded in red when across the optic nerve or blue when across the injection site. (**C**) Left panels: spidergrams of the ONL thickness of *Rho*$^{P23H/+}$ mice injected with mOP-ctrl (red), mOP-*shEgr1* (blue), or mOP-*mEgr1* (green) at 4, 8 and 12 wpi. Measurements were taken every 200 µm from the optic nerve head (0 µm). Shown are means and range of n=4–9. Right panels: quantification of the ONL thickness of the nasal (transduced) retina after AAV injections. Data points show the average ONL thickness of all retinas at ten positions (400 µm to 2200 µm; 200 µm intervals) in the nasal retina. Shown are means ± SD. One-way ANOVA with Tukey's multiple comparisons test, p values as indicated. **D**) Same samples as in (C) but analyzed differently to reflect the progression of degeneration for each type of AAV throughout time. The data points represent the averages of all measurements taken in the nasal ONL for each individual sample; thus, each point on the bar graph corresponds to one retina analyzed. Two-way ANOVA with Tukey's multiple comparisons test, p values as indicated. n=4–9. ONL: outer nuclear layer; INL: inner nuclear layer; GCL: ganglion cell layer.

Targeted modulation of Egr1 in cones of wild-type mice: To investigate the transduction and expression profile of the cone-specific AAVs driven by the human *OPN1MW* gene promoter, the vectors were injected into the subretinal space of 4-week-old wt mice. In vivo analysis was performed via funduscopy and OCT imaging at 8 wpi. As observed with the rod-specific vectors, minor disturbances to retinal layers at the injection sites were visible by OCT (Figure 5A-C, arrows and blue lines and squares), but the overall structure of the retina was preserved, as indicated by OCT scans across the optic nerve (red lines and squares). Widespread viral transduction was detected via fluorescent funduscopy. GFP fluorescence in retinal sections confirmed expression in cells almost exclusively at the outer rim of the ONL, suggesting specificity for cones, which was verified by co-staining with PNA. Only sparse EGR1 staining was detected in AAV::*OPN1MW-shEgr1* injected retinas (Figure 5B, bottom row), while increased EGR1 signals were evident in PNA-positive cells at the outer rim of the ONL in AAV::*OPN1MW-mEgr1* injected mice (Figure 5C, bottom row). Since a potential toxic effect on cone photoreceptors cannot be detected by measuring the thickness of the ONL, we compared the number of cones across treatments and between transduced and untransduced retinal areas by counting ARR3-positive cells (Figure 5D, left). Results showed that neither up- nor downregulation of *Egr1* in cones of wt mice affected the number of cones at 8 wpi (Figure 5D, right).

Cones of Rho$^{P23H/+}$ mice are not affected by the modulation of Egr1 expression: Although cones are not directly affected in RP models, they degenerate secondarily for reasons still not well understood. To investigate a potential role of EGR1

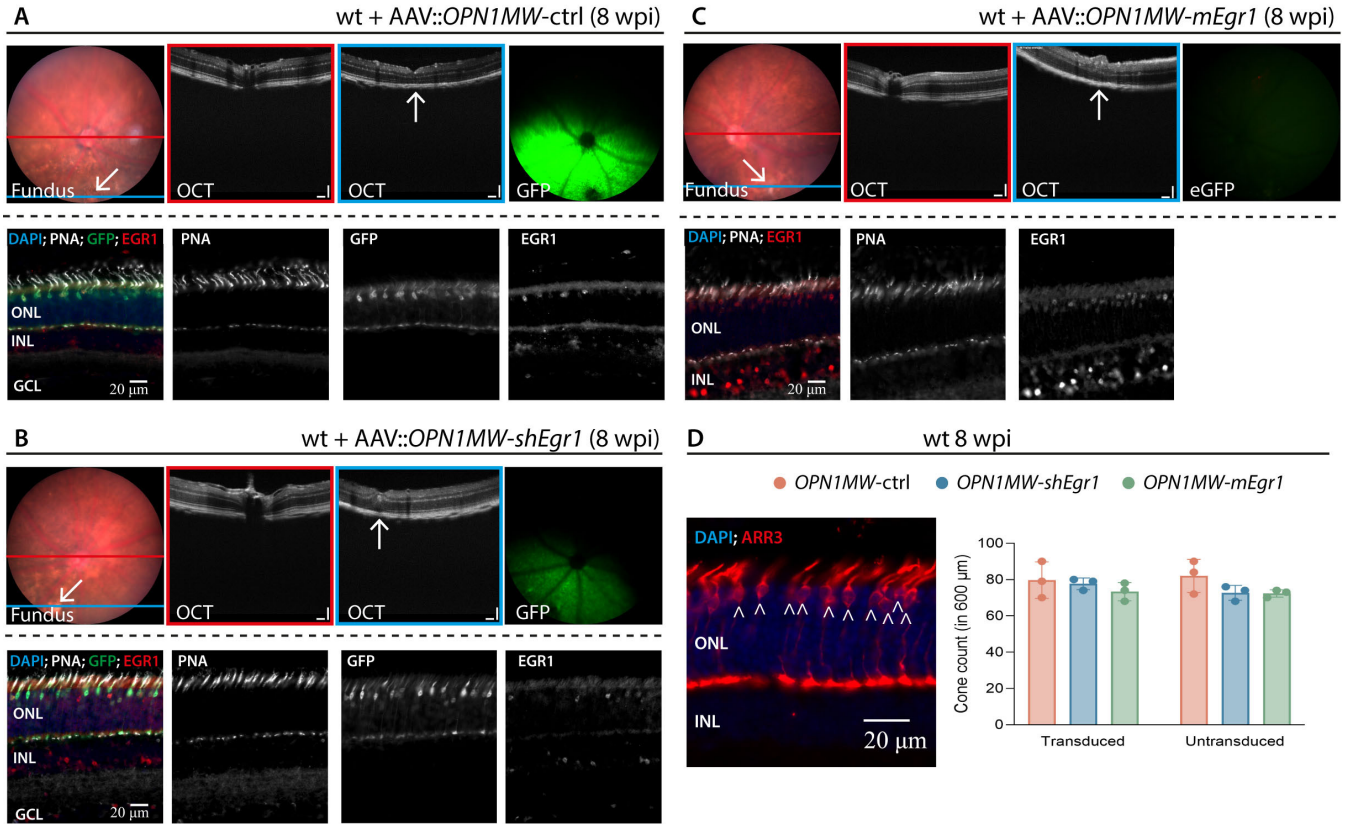

Figure 5. Expression and safety of *shEgr1* and *mEgr1* transgenes in wt cones. (**A-C**) Fundus images and OCT scans (top rows) and immunofluorescence images (bottom rows) of wt retinas subretinally injected with **(A)** AAV::*OPN1MW*-ctrl, **(B)** AAV::*OPN1MW-shEgr1* and **(C)** AAV::*OPN1MW-mEgr1* at 8 wpi. White arrows point to injection sites. OCT scans are color-coded in red when across the optic nerve or blue when across the injection site. Immunofluorescence panels show the transduction pattern of the virus (GFP, except AAV::*OPN1MW-mEgr1*) as well as EGR1 and PNA-positive cells as grayscale images and the colored merge. Scale bars: 20 µm. **D**) Left panel: example image of a cone arrestin (ARR3) staining in wt mice. Right panel: bar graph reporting the number of ARR3-positive cells in a 600 µm-long region of the transduced and untransduced retinal areas of wt mice at 8 wpi of AAV::mOP-ctrl (red), AAV::mOP-*shEgr1* (blue), and AAV::mOP-*mEgr1* (green). Shown are individual values and the mean ± SD. Two-way ANOVA with Šídák's multiple comparisons test. n=3. ONL: outer nuclear layer; INL: inner nuclear layer; GCL: ganglion cell layer.

in cone survival in the context of primary rod degeneration, we injected the cone-specific vectors in 4-week-old *Rho*$^{P23H/+}$ mice. Fundus and OCT images at 8 wpi did not reveal notable differences across treatments (Figure 6A-C, top rows). Immunofluorescence showed targeted expression of the vectors in *Rho*$^{P23H/+}$ cones and apparently reduced EGR1 signals in AAV-*OPN1MW-shEgr1* retinas (Figure 6B, bottom row). Transduction with AAV::*OPN1MW-mEgr1* did not notably increase EGR1 expression over control, as most (if not all) cones in the *Rho*$^{P23H/+}$ retina already expressed the transcription factor (Figure 6A,C; bottom rows). To directly assess the effects of EGR1 on cones in the degenerative model, we quantified surviving ARR3-positive cones (Figure 6D, left) and compared their number across treatments and in transduced versus untransduced areas. Data showed that modulation of *Egr1* expression in cones of the *Rho*$^{P23H/+}$ mouse did not influence their survival (Figure 6D, right).

DISCUSSION

A hallmark of a cell's response to different environmental and physiologic stimuli is the rapid modulation of gene expression, often mediated by immediate early genes (IEGs) such as EGR1, which is frequently upregulated in photoreceptors during the early phase of retinal degeneration. The available evidence points to EGR1 as a possible unifying feature in dying photoreceptors, although its functional role in the degenerative process remains to be elucidated. In this research we used AAV-based RNAi and transgenic overexpression to modulate *Egr1* levels in dying photoreceptors of *Rho*$^{P23H/+}$ mice. The *Rho*$^{P23H/+}$ mouse model is one of

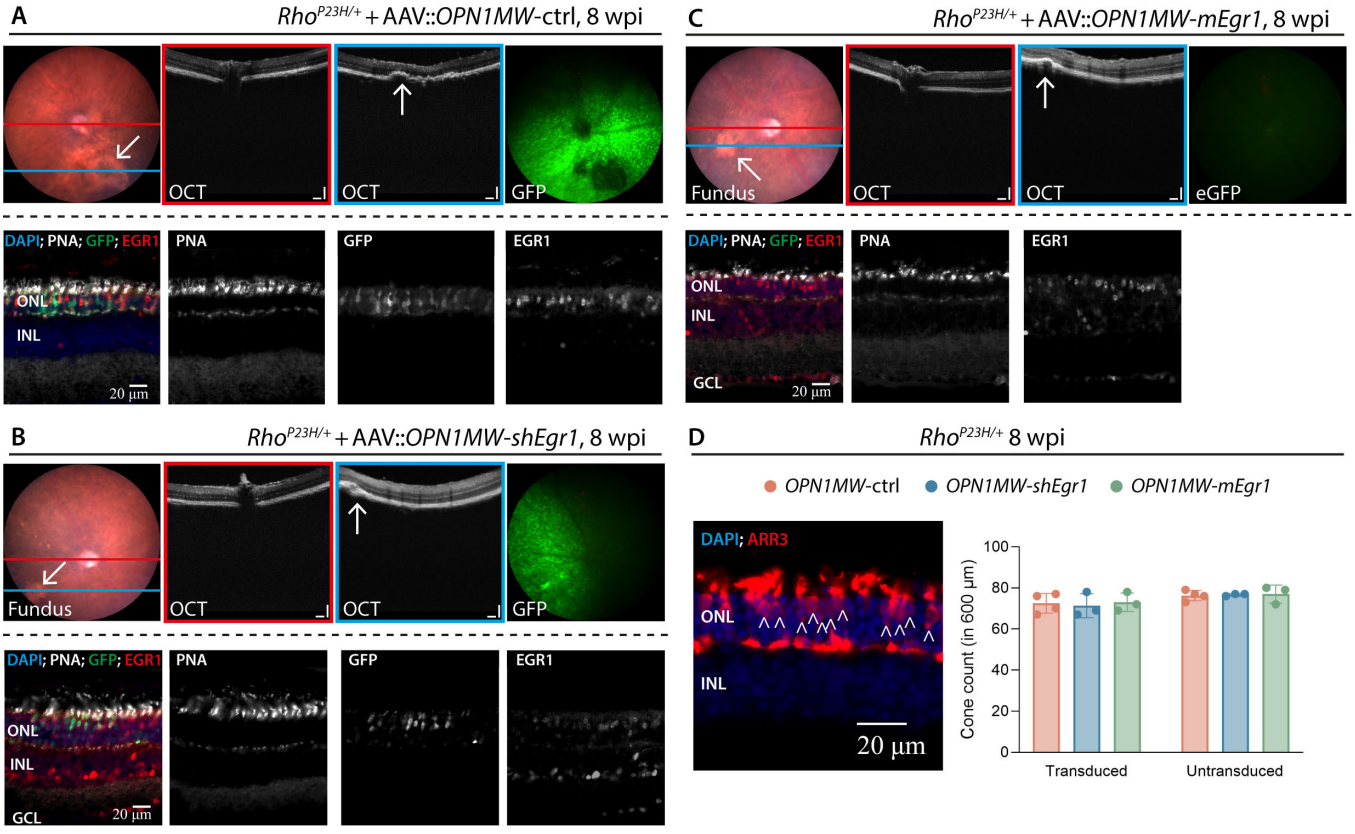

Figure 6. Phenotypic evaluation of *OPN1MW*-driven AAVs in *Rho*$^{P23H/+}$ mice. **A-C**: Fundus images, OCT scans (top rows), and immunofluorescence images (bottom rows) of *Rho*$^{P23H/+}$ retinas subretinally injected with **(A)** AAV::*OPN1MW*-ctrl, **(B)** AAV::*OPN1MW-shEgr1* and (**C**) AAV::*OPN1MW-mEgr1* at 8 wpi. White arrows point to injection sites. OCT scans are color-coded in red when across the optic nerve or blue when across the injection site. Immunofluorescence panels show the transduction pattern of the virus (GFP, except AAV-*OPN1MW*-mEgr1 as well as EGR1 and PNA-positive cells as grayscale images and the colored merge. Scale bars: 20 µm. (**D**) Left panel: example image of a cone arrestin (ARR3) staining in *Rho*$^{P23H/+}$ mice. Right panel: bar graph reporting the number of ARR3-positive cells in a 600 µm-long section of the transduced and untransduced retinal areas of *Rho*$^{P23H/+}$ mice at 8 wpi of AAV::mOP-ctrl (red), AAV::mOP-*shEgr1* (blue), and AAV::mOP-*mEgr1* (green). Shown are individual values and means ± SD. Two-way ANOVA with Šídák's multiple comparisons test. n=3–4. ONL: outer nuclear layer; INL: inner nuclear layer; GCL: ganglion cell layer.

the most widely used and well characterized genetic models for studying retinal degeneration. The main advantage is its clinical relevance, as the mutation is frequently found in RP patients, and it mimics the slow progressive loss of rod photoreceptors, followed by secondary cone death. The slow degenerative process also offers a wider time window that is required for treatment approaches using AAV-mediated genetic manipulations.

Our study contributes to a complex research landscape on the function of EGR1 in the retina, since previous reports have yielded conflicting findings about its role in retinal degeneration. In the retinoschisis mouse, *Egr1* was not necessary to trigger cell death processes, despite its massive upregulation during early stages of degeneration [37,38]. Sharma and colleagues suggested that *Egr1* might actually serve a protective function in the rds model [39]. Quite the opposite was reported by Dong and colleagues ten years later, pointing to a positive correlation between *Egr1* expression and degenerative processes [40]. In an attempt to resolve the functions of EGR1, we manipulated its levels in rods and cones of wt and *Rho*$^{P23H/+}$ mice. Our data indicate that increased endogenous expression of *Egr1* in rods may contribute to disease progression as its downregulation slowed the loss of rod photoreceptors in *Rho*$^{P23H/+}$ mice. Since the protective effect was only moderate and did not fully rescue the phenotype, our data suggest that *Egr1* may function as a signaling molecule rather than a causative factor for rod degeneration. One potential explanation for the modest effect of the *Egr1* knockdown is a certain redundancy within the EGR transcription factor family. Although not directly tested in our model, it is possible that *Egr2, Egr3*, and/or *Egr4* provided compensatory activity when *Egr1* was reduced [66,67]. Surprisingly, *Egr1* overexpression did not produce the opposite effect to the *Egr1* knockdown. We hypothesize that the lack of effect after EGR1 overexpression may be due to a "ceiling effect": the degenerating retina already exhibits high EGR1 activation, and thus additional overexpression may not further increase its activity as the system may be saturated.

Modulation of *Egr1* expression in rods or cones of the healthy retina had no significant effect, which excludes EGR1 as a causative death factor. Possibly, EGR1 exerts its function only in connection to a noxious stimulus that triggers the degeneration. Indeed, it has been reported that genes (or genetic variations [68]) that do not cause cell stress or are even beneficial in a normal situation become harmful when combined with an environmental trigger, a concept known as gene-environment interaction [69]. One example is the soluble peptide sAPPα (amyloid precursor protein alpha). On one hand, the peptide can promote physiologic brain functions and neuroprotection [70]; on the other hand, the protein overabundance caused by a toxic stimulus (i.e., brain ischemia or inflammation) can lead to tumorigenesis [71]. Another prominent example is p53, whose regulation is, at least partially, controlled by EGR1 [26]. Under conditions of moderate stress, p53 elicits protective responses, such as temporary cell-cycle arrest, DNA repair, and antioxidant protein production, to maintain genomic homeostasis in cells that sustain reparable damage [72]. However, in cells exposed to potent stress signals, p53 drives irreversible programs of apoptosis to reduce the number of malignant cells [73].

To fully unravel the function of EGR1 in the degenerating retina, it is important to identify the mechanisms that regulate *Egr1* expression in situations of cellular stress. A hallmark of retinal degeneration is the early disintegration of the photoreceptor outer segments, creating a mechanical stress on the cell. Since mechanical stress has been implicated in the activation of EGR1 in cultured epithelial cells via MAPK signaling acting on the serum response elements (SREs) on the *Egr1* promoter [15,74-76], it is possible that *Egr1* expression is activated by early structural alterations in the delicate cytoskeletal structure of the photoreceptor cell. The moderate protection conferred by silencing *Egr1* in rods may indicate that the activation of the transcription factor in a degenerative state might modulate the injured cell's transcriptional response, preparing it for degeneration. Such a process may be beneficial for the complex retinal tissue as it removes nonfunctional cells that may interfere with the function of the tissue. Interestingly, and maybe in support of this, we identified several genes encoding tubulin cytoskeleton-associated proteins as putative targets for EGR1 through single-cell RNA sequencing [44] of the degenerating rd10 retina. These gene products may facilitate the morphological alterations in the cytoskeleton that are needed for a controlled cell death and the removal of cellular debris by microglia or other phagocytosing cells. Clearly, investigations into DNA–protein interactions using ChiP-seq and/or CUT&RUN [77,78] assays will be helpful to shed more light on EGR1 targets, hopefully allowing a more detailed description of its function during degenerative processes in the future.

CONCLUSIONS: The aim of this work was to define the function of *Egr1* in the context of retinal degeneration, addressing the current scarcity of in vivo data despite its implication in various retinal disorders. Our data indicate that *Egr1* moderately promotes the development and/or progression of rod degeneration but may not be the primary driver of the disease. However, the precise function of EGR1 in photoreceptor

degeneration remains unclear until the activating signal(s) and downstream targets are identified.

ACKNOWLEDGMENTS

Ethics approval Animal experimentation was approved by the authorities of the Kanton Zürich (license numbers: ZH019/2019 and ZH105/2022) and adhered to the ARVO statement for the use of Animals in Ophthalmic and Vision Research. Competing interests: The authors declare no competing interests. Funding: This work was supported by the Swiss National Science Foundation (grant number 310030_200798). Data availability: The authors confirm that the data supporting this study are available within the article. Raw data can be shared by the corresponding authors upon reasonable request. Authors' contributions: LM, MS, and CG conceived the study and contributed to data interpretation. LM, AF, CI, CM, LPG, MS, JR, MN performed experiments and contributed material. LM analyzed the data. LM and CG wrote the manuscript. All authors red and approved the final manuscript. Dr. Luca Merolla (luca.merolla@uzh.ch) and Dr. Christian Grimm (cgrimm@opht.uzh.ch) are co-corresponding authors for this paper. We thank the Laboratory Animal Services Centre (LASC) of the University of Zurich for animal care.

REFERENCES

1. Sorrentino FS, Gallenga CE, Bonifazzi C, Perri P. A challenge to the striking genotypic heterogeneity of retinitis pigmentosa: a better understanding of the pathophysiology using the newest genetic strategies. Eye (Lond) 2016; 30:1542-8. [PMID: 27564722].

2. Verbakel SK, van Huet RAC, Boon CJF, den Hollander AI, Collin RWJ, Klaver CCW, Hoyng CB, Roepman R, Klevering BJ. Non-syndromic retinitis pigmentosa. Prog Retin Eye Res 2018; 66:157-86. [PMID: 29597005].

3. Dryja TP, McGee TL, Reichel E, Hahn LB, Cowley GS, Yandell DW, Sandberg MA, Berson EL. A point mutation of the rhodopsin gene in one form of retinitis pigmentosa. Nature 1990; 343:364-6. [PMID: 2137202].

4. Sohocki MM, Daiger SP, Bowne SJ, Rodriquez JA, Northrup H, Heckenlively JR, Birch DG, Mintz-Hittner H, Ruiz RS, Lewis RA, Saperstein DA, Sullivan LS. Prevalence of mutations causing retinitis pigmentosa and other inherited retinopathies. Hum Mutat 2001; 17:42-51. [PMID: 11139241].

5. Vasudevan S, Senapati S, Pendergast M, Park PSH. Aggregation of rhodopsin mutants in mouse models of autosomal dominant retinitis pigmentosa. Nat Commun 2024; 15:1451- [PMID: 38365903].

6. Sakami S, Maeda T, Bereta G, Okano K, Golczak M, Sumaroka A, Roman AJ, Cideciyan AV, Jacobson SG, Palczewski K. Probing mechanisms of photoreceptor degeneration in a new mouse model of the common form of autosomal dominant retinitis pigmentosa due to P23H opsin mutations. J Biol Chem 2011; 286:10551-67. [PMID: 21224384].

7. Green ES, Menz MD, LaVail MM, Flannery JG. Characterization of rhodopsin mis-sorting and constitutive activation in a transgenic rat model of retinitis pigmentosa. Invest Ophthalmol Vis Sci 2000; 41:1546-53. [PMID: 10798675].

8. Liu X, Wu T-H, Stowe S, Matsushita A, Arikawa K, Naash MI, Williams DS. Defective phototransductive disk membrane morphogenesis in transgenic mice expressing opsin with a mutated N-terminal domain. J Cell Sci 1997; 110:2589-97. [PMID: 9372448].

9. Bahrami S, Drabløs F. Gene regulation in the immediate-early response process. Adv Biol Regul 2016; 62:37-49. [PMID: 27220739].

10. Cao XM, Koski RA, Gashler A, McKiernan M, Morris CF, Gaffney R, Hay RV, Sukhatme VP. Identification and characterization of the Egr-1 gene product, a DNA-binding zinc finger protein induced by differentiation and growth signals. Mol Cell Biol 1990; 10:1931-9. [PMID: 2109185].

11. Müller I, Lipp P, Thiel G. Ca2+ signaling and gene transcription in glucose-stimulated insulinoma cells. Cell Calcium 2012; 52:137-51. [PMID: 22658828].

12. Trinh N-T, Yamashita T, Ohneda K, Kimura K, Salazar GT, Sato F, Ohneda O. Salazar GTa, Sato F, Ohneda O. Increased expression of EGR-1 in diabetic human adipose tissue-derived mesenchymal stem cells reduces their wound healing capacity. Stem Cells Dev 2016; 25:760-73. [PMID: 26988763].

13. Huang RP, Fan Y, Boynton AL. UV irradiation upregulates Egr-1 expression at transcription level. J Cell Biochem 1999; 73:227-36. [PMID: 10227386].

14. Huang RP, Fan Y, deBelle I, Ni Z, Matheny W, Adamson ED. Egr-1 inhibits apoptosis during the UV response: correlation of cell survival with Egr-1 phosphorylation. Cell Death Differ 1998; 5:96-106. [PMID: 10200450].

15. Kwon T, Leroux A-C, Zang H, Pollard D, Zehe C, Akbari S. Cell-based shear stress sensor for bioprocessing. J Biotechnol 2024; 390:71-9. [PMID: 38685415].

16. Qin X, Jiang Y, Tse YC, Wang Y, Wong TP, Paudel HK. Early Growth Response 1 (Egr-1) Regulates N-Methyl-d-aspartate Receptor (NMDAR)-dependent Transcription of PSD-95 and α-Amino-3-hydroxy-5-methyl-4-isoxazole Propionic Acid Receptor (AMPAR) Trafficking in Hippocampal Primary Neurons. J Biol Chem 2015; 290:29603-16. [PMID: 26475861].

17. Heynen AJ, Bear MF. Long-term potentiation of thalamocortical transmission in the adult visual cortex in vivo. J Neurosci 2001; 21:9801-13. [PMID: 11739588].

18. Shan Y, Carlock LR, Walker PD. NMDA receptor overstimulation triggers a prolonged wave of immediate early gene expression: relationship to excitotoxicity. Exp Neurol 1997; 144:406-15. [PMID: 9168840].

19. Cole AJ, Saffen DW, Baraban JM, Worley PF. Rapid increase of an immediate early gene messenger RNA in hippocampal neurons by synaptic NMDA receptor activation. Nature 1989; 340:474-6. [PMID: 2547165].

20. Mo J, Kim C-H, Lee D, Sun W, Lee HW, Kim H. Early growth response 1 (Egr-1) directly regulates GABAA receptor α2, α4, and θ subunits in the hippocampus. J Neurochem 2015; 133:489-500. [PMID: 25708312].

21. Jones MW, Errington ML, French PJ, Fine A, Bliss TV, Garel S, Charnay P, Bozon B, Laroche S, Davis S. A requirement for the immediate early gene Zif268 in the expression of late LTP and long-term memories. Nat Neurosci 2001; 4:289-96. [PMID: 11224546].

22. Myung E, Park Y-L, Kim N, Chung C-Y, Park H-B, Park H-C, Myung D-S, Kim J-S, Cho S-B, Lee W-S, Joo YE. Expression of early growth response-1 in human gastric cancer and its relationship with tumor cell behaviors and prognosis. Pathol Res Pract 2013; 209:692-9. [PMID: 24011795].

23. Gabriel KN, Jones AC, Nguyen JP, Antillon KS, Janos SN, Overton HN, Jenkins SM, Frisch EH, Trujillo KA, Bisoffi M. Association and regulation of protein factors of field effect in prostate tissues. Int J Oncol 2016; 49:1541-52. [PMID: 27634112].

24. Li L, Ameri AH, Wang S, Jansson KH, Casey OM, Yang Q, Beshiri ML, Fang L, Lake RG, Agarwal S, Alilin AN, Xu W, Yin J, Kelly K. EGR1 regulates angiogenic and osteoclastogenic factors in prostate cancer and promotes metastasis. Oncogene 2019; 38:6241-55. [PMID: 31312026].

25. Ma Z, Gao X, Shuai Y, Wu X, Yan Y, Xing X, Ji J. EGR1-mediated linc01503 promotes cell cycle progression and tumorigenesis in gastric cancer. Cell Prolif 2021; 54:e12922[PMID: 33145887].

26. Baron V, Adamson ED, Calogero A, Ragona G, Mercola D. The transcription factor Egr1 is a direct regulator of multiple tumor suppressors including TGFbeta1, PTEN, p53, and fibronectin. Cancer Gene Ther 2006; 13:115-24. [PMID: 16138117].

27. Ashby R, Kozulin P, Megaw PL, Morgan IG. Alterations in ZENK and glucagon RNA transcript expression during increased ocular growth in chickens. Mol Vis 2010; 16:639-49. [PMID: 20405027].

28. Bitzer M, Schaeffel F. Defocus-induced changes in ZENK expression in the chicken retina. Invest Ophthalmol Vis Sci 2002; 43:246-52. [PMID: 11773038].

29. Zhang L, Cho J, Ptak D, Leung YF. The role of egr1 in early zebrafish retinogenesis. PLoS One 2013; 8:e56108[PMID: 23405257].

30. Fischer AJ, Scott MA, Tuten W. Mitogen-activated protein kinase-signaling stimulates Müller glia to proliferate in acutely damaged chicken retina. Glia 2009; 57:166-81. [PMID: 18709648].

31. Schippert R, Burkhardt E, Feldkaemper M, Schaeffel F. Relative axial myopia in Egr-1 (ZENK) knockout mice. Invest Ophthalmol Vis Sci 2007; 48:11-7. [PMID: 17197510].

32. Humphries A, Carter DA. Circadian dependency of nocturnal immediate-early protein induction in rat retina. Biochem Biophys Res Commun 2004; 320:551-6. [PMID: 15219864].

33. Agarwal N. Diurnal expression of NGF1-A mRNA in retinal degeneration slow (rds) mutant mouse retina. FEBS Lett 1994; 339:253-7. [PMID: 8112464].

34. Brand C, Burkhardt E, Schaeffel F, Choi JW, Feldkaemper MP. Regulation of Egr-1, VIP, and Shh mRNA and Egr-1 protein in the mouse retina by light and image quality. Mol Vis 2005; 11:309-20. [PMID: 15889015].

35. Simon P, Schott K, Williams RW, Schaeffel F. Posttranscriptional regulation of the immediate-early gene EGR1 by light in the mouse retina. Eur J Neurosci 2004; 20:3371-7. [PMID: 15610169].

36. Merolla L, Samardzija M, Kostic C, Grimm C. Photoreceptor activation drives the expression of the immediate-early gene Egr1 in inner retinal neurons. Exp Eye Res 2025; 260:110602[PMID: 40876616].

37. Gehrig A, Langmann T, Horling F, Janssen A, Bonin M, Walter M, Poths S, Weber BHF. Genome-wide expression profiling of the retinoschisin-deficient retina in early postnatal mouse development. Invest Ophthalmol Vis Sci 2007; 48:891-900. [PMID: 17251492].

38. Langmann T, Ebert S, Walczak Y, Weigelt K, Ehrengruber MU, Stiewe T, Weber BHF. Induction of early growth response-1 mediates microglia activation in vitro but is dispensable in vivo. Neuromolecular Med 2009; 11:87-96. [PMID: 19365618].

39. Sharma YV, Cojocaru RI, Ritter LM, Khattree N, Brooks M, Scott A, Swaroop A, Goldberg AFX. Protective gene expression changes elicited by an inherited defect in photoreceptor structure. PLoS One 2012; 7:e31371[PMID: 22363631].

40. Dong Y, Xu W, Li Y, Wei C, Hu Y, Hu Z, Paquet-Durand F, Jiao K. Inhibition of the MAPK/c-Jun-EGR1 Pathway Decreases Photoreceptor Cell Death in the rd1 Mouse Model for Inherited Retinal Degeneration. Int J Mol Sci 2022; 23:.

41. Sahaboglu A, Sharif A, Feng L, Secer E, Zrenner E, Paquet-Durand F. Temporal progression of PARP activity in the Prph2 mutant rd2 mouse: Neuroprotective effects of the PARP inhibitor PJ34. PLoS One 2017; 12:e0181374[PMID: 28723922].

42. Kaur J, Mencl S, Sahaboglu A, Farinelli P, van Veen T, Zrenner E, Ekström P, Paquet-Durand F, Arango-Gonzalez B. Calpain and PARP activation during photoreceptor cell death in P23H and S334ter rhodopsin mutant rats. PLoS One 2011; 6:e22181[PMID: 21765948].

43. Jiao K, Sahaboglu A, Zrenner E, Ueffing M, Ekström PA, Paquet-Durand F. Efficacy of PARP inhibition in Pde6a mutant mouse models for retinitis pigmentosa depends on the quality and composition of individual human mutations. Cell Death Discov 2016; 2:16040-[PMID: 27551530].

44. Karademir D, Todorova V, Ebner LJA, Samardzija M, Grimm C. Single-cell RNA sequencing of the retina in a model

of retinitis pigmentosa reveals early responses to degeneration in rods and cones. BMC Biol 2022; 20:86-[PMID: 35413909].

45. . de Brito e Cunha D. Frederico ABT, Azamor T, Melgaço JG, da Costa Neves PC, Bom APDA, Tilli TM, Missailidis S. Biotechnological Evolution of siRNA Molecules: From Bench Tool to the Refined Drug. Pharmaceuticals 2022; 15:575-.

46. Fellmann C, Hoffmann T, Sridhar V, Hopfgartner B, Muhar M, Roth M, Lai DY, Barbosa IAM, Kwon JS, Guan Y, Sinha N, Zuber J. An optimized microRNA backbone for effective single-copy RNAi. Cell Rep 2013; 5:1704-13. [PMID: 24332856].

47. Lee Y, Ahn C, Han J, Choi H, Kim J, Yim J, Lee J, Provost P, Rådmark O, Kim S, Kim VN. The nuclear RNase III Drosha initiates microRNA processing. Nature 2003; 425:415-9. [PMID: 14508493].

48. Silva JM, Li MZ, Chang K, Ge W, Golding MC, Rickles RJ, Siolas D, Hu G, Paddison PJ, Schlabach MR, Sheth N, Bradshaw J, Burchard J, Kulkarni A, Cavet G, Sachidanandam R, McCombie WR, Cleary MA, Elledge SJ, Hannon GJ. Second-generation shRNA libraries covering the mouse and human genomes. Nat Genet 2005; 37:1281-8. [PMID: 16200065].

49. Reid CA, Ertel KJ, Lipinski DM. Improvement of Photoreceptor Targeting via Intravitreal Delivery in Mouse and Human Retina Using Combinatory rAAV2 Capsid Mutant Vectors. Invest Ophthalmol Vis Sci 2017; 58:6429-39. [PMID: 29260200].

50. Dalkara D, Byrne LC, Klimczak RR, Visel M, Yin L, Merigan WH, Flannery JG, Schaffer DV. In vivo-directed evolution of a new adeno-associated virus for therapeutic outer retinal gene delivery from the vitreous. Sci Transl Med 2013; 5:189ra76[PMID: 23761039].

51. Barborek R, Rowlan J, Kuchenbecker J, Rezeanu D, Mazzaferri M, Bembry B, Rojas J, Tang Y, Romano C, Neitz J, Neitz M. An AAV vector carrying a chimeric photopigment for evaluating gene therapy methods in Old World primates. Invest Ophthalmol Vis Sci 2021; 62:2785-.

52. Beltran WA, Boye SL, Boye SE, Chiodo VA, Lewin AS, Hauswirth WW, Aguirre GD. rAAV2/5 gene-targeting to rods:dose-dependent efficiency and complications associated with different promoters. Gene Ther 2010; 17:1162-74. [PMID: 20428215].

53. Choudhary M, Tayyari F, Handa JT, Malek G. Characterization and identification of measurable endpoints in a mouse model featuring age-related retinal pathologies: a platform to test therapies. Lab Invest 2022; 102:1132-42. [PMID: 35589984].

54. Mattapallil MJ, Wawrousek EF, Chan CC, Zhao H, Roychoudhury J, Ferguson TA, Caspi RR. The Rd8 mutation of the Crb1 gene is present in vendor lines of C57BL/6N mice and embryonic stem cells, and confounds ocular induced mutant phenotypes. Invest Ophthalmol Vis Sci 2012; 53:2921-7. [PMID: 22447858].

55. Tan E, Ding XQ, Saadi A, Agarwal N, Naash MI, Al-Ubaidi MR. Expression of cone-photoreceptor-specific antigens in a cell line derived from retinal tumors in transgenic mice. Invest Ophthalmol Vis Sci 2004; 45:764-8. [PMID: 14985288].

56. Yu J, de Belle I, Liang H, Adamson ED. Coactivating factors p300 and CBP are transcriptionally crossregulated by Egr1 in prostate cells, leading to divergent responses. Mol Cell 2004; 15:83-94. [PMID: 15225550].

57. Barben M, Schori C, Samardzija M, Grimm C. Targeting Hif1a rescues cone degeneration and prevents subretinal neovascularization in a model of chronic hypoxia. Mol Neurodegener 2018; 13:12-[PMID: 29514656].

58. Grimm C, Remé CE. Light damage as a model of retinal degeneration. Methods Mol Biol 2013; 935:87-97. [PMID: 23150362].

59. Livak KJ, Schmittgen TD. Analysis of relative gene expression data using real-time quantitative PCR and the 2(-Delta Delta C(T)) Method. Methods 2001; 25:402-8. [PMID: 11846609].

60. Iwasaki M, Myers KM, Rayborn ME, Hollyfield JG. Interphotoreceptor matrix in the human retina: cone-like domains surround a small population of rod photoreceptors. J Comp Neurol 1992; 319:277-84. [PMID: 1387887].

61. Morita K, Ebert SN, Wong DL. Role of transcription factor Egr-1 in phorbol ester-induced phenylethanolamine N-methyltransferase gene expression. J Biol Chem 1995; 270:11161-7. [PMID: 7744747].

62. Bottone FG Jr, Moon Y, Alston-Mills B, Eling TE. Transcriptional regulation of activating transcription factor 3 involves the early growth response-1 gene. J Pharmacol Exp Ther 2005; 315:668-77. [PMID: 16079301].

63. Mayer SI, Dexheimer V, Nishida E, Kitajima S, Thiel G. Expression of the transcriptional repressor ATF3 in gonadotrophs is regulated by Egr-1, CREB, and ATF2 after gonadotropin-releasing hormone receptor stimulation. Endocrinology 2008; 149:6311-25. [PMID: 18719024].

64. Rashid MU, Coombs KM. Serum-reduced media impacts on cell viability and protein expression in human lung epithelial cells. J Cell Physiol 2019; 234:7718-24. [PMID: 30515823].

65. Geiger F, Heigl T, Merolla L, Yong M, Wögenstein GM, Govers LP, Tsioti I, Fottner A, Samardzija M, Grimm C. HIF1 activity in photoreceptors drives type 3 neovascularization and retinal atrophy in a new mouse model of age-related macular degeneration. Cell Death Dis 2025; 16:687-[PMID: 41053106].

66. O'Donovan KJ, Tourtellotte WG, Millbrandt J, Baraban JM. The EGR family of transcription-regulatory factors: progress at the interface of molecular and systems neuroscience. Trends Neurosci 1999; 22:167-73. [PMID: 10203854].

67. Tourtellotte WG, Nagarajan R, Bartke A, Milbrandt J. Functional compensation by Egr4 in Egr1-dependent luteinizing hormone regulation and Leydig cell steroidogenesis. Mol Cell Biol 2000; 20:5261-8. [PMID: 10866682].

68. McDermott R, Tingley D, Cowden J, Frazzetto G, Johnson DDP. Monoamine oxidase A gene (MAOA) predicts behavioral aggression following provocation. Proc Natl Acad Sci U S A 2009; 106:2118-23. [PMID: 19168625].

69. Virolainen SJ, VonHandorf A, Viel KCMF, Weirauch MT, Kottyan LC. Gene-environment interactions and their impact on human health. Genes Immun 2023; 24:1-11. [PMID: 36585519].

70. Chasseigneaux S, Allinquant B. Functions of Aβ, sAPPα and sAPPβ : similarities and differences. J Neurochem 2012; 120:Suppl 199-108. [PMID: 22150401].

71. Nhan HS, Chiang K, Koo EH. The multifaceted nature of amyloid precursor protein and its proteolytic fragments: friends and foes. Acta Neuropathol 2015; 129:1-19. [PMID: 25287911].

72. Brady CA, Attardi LD. p53 at a glance. J Cell Sci 2010; 123:2527-32. [PMID: 20940128].

73. Vousden KH, Prives C. Blinded by the Light: The Growing Complexity of p53. Cell 2009; 137:413-31. [PMID: 19410540].

74. Khachigian LM, Anderson KR, Halnon NJ, Gimbrone MA Jr, Resnick N, Collins T. Egr-1 is activated in endothelial cells exposed to fluid shear stress and interacts with a novel shear-stress-response element in the PDGF A-chain promoter. Arterioscler Thromb Vasc Biol 1997; 17:2280-6. [PMID: 9351401].

75. Tseng H, Peterson TE, Berk BC. Fluid shear stress stimulates mitogen-activated protein kinase in endothelial cells. Circ Res 1995; 77:869-78. [PMID: 7554140].

76. Havis E, Duprez D. EGR1 Transcription Factor is a Multifaceted Regulator of Matrix Production in Tendons and Other Connective Tissues. Int J Mol Sci 2020; 21:1664-[PMID: 32121305].

77. Skene PJ, Henikoff S. An efficient targeted nuclease strategy for high-resolution mapping of DNA binding sites. Elife 2017; 6:6-[PMID: 28079019].

78. Skene PJ, Henikoff JG, Henikoff S. Targeted in situ genome-wide profiling with high efficiency for low cell numbers. Nat Protoc 2018; 13:1006-19. [PMID: 29651053].

Articles are provided courtesy of Emory University and The Abraham J. & Phyllis Katz Foundation. The print version of this article was created on 20 February 2026. This reflects all typographical corrections and errata to the article through that date. Details of any changes may be found in the online version of the article.